Research Square

Preprints are preliminary reports that have not undergone peer review.
They should not be considered conclusive, used to inform clinical practice,
or referenced by the media as validated information.

Selective Iron Extraction and Ti–V Distribution from Magnetite–Ilmenite Iron Sand via Carbothermic Reduction and Magnetic Separation

Elnando Latuputty
University of Indonesia
M. Faris Fadillah
Sumatera Institute of Technology
La Ode Arham
Sumatera Institute of Technology
Bambang Suharno
prof.suharno@gmail.com
University of Indonesia
Yuliana Sari
University of Indonesia
Suharto Suharto
National Research and Innovation Agency
Fajar Nurjaman
National Research and Innovation Agency

Research Article

Keywords: Iron Sand, Carbothermic Reduction, Magnetic Separation, Fe-Ti-V

Posted Date: November 25th, 2026

DOI: https://doi.org/10.21203/rs.3.rs-11755939/v1

License: This work is licensed under a Creative Commons Attribution 4.0 International License.
Read Full License

Additional Declarations: No competing interests reported.

Selective Iron Extraction and Ti–V Distribution from Magnetite–Ilmenite Iron Sand via Carbothermic Reduction and Magnetic Separation

Elnando Latuputty[1,3]*, M. Faris Fadillah[2], La Ode Arham[2], Bambang Suharno[1]*, Yuliana Sari[1,3], Suharto Suharto[3], and Fajar Nurjaman[3]

Affiliations

[1] Department of Metallurgical Engineering and Materials, Faculty of Engineering, Universitas Indonesia, Depok 16425, Indonesia,

[2] Study Program of Mining Engineering, Faculty of Technology Industries, Institute Technology of Sumatera, South Lampung, Indonesia,

[3] Research Center for Mineral Technology, National Research and Innovation Agency, South Lampung 35361, Indonesia.

*Corresponding author: prof.suharno@gmail.com, elnandoisaac@gmail.com

Abstract

Low-grade iron sand contains iron (Fe), titanium (Ti), and vanadium (V), but their selective recovery is challenging because iron oxides are closely associated with silicate and titanate minerals. This study aimed to optimize coal dosage, reduction temperature, and holding time during carbothermic reduction followed by magnetic separation, and to investigate how mineral phase transformations and metallic iron grain growth affect Fe recovery and Ti–V partitioning. Coal dosage was varied from 10 to 30 wt.% relative to ore mass, reduction temperature from 1000 to 1200 °C, and holding time from 30 to 120 min. X-ray fluorescence (XRF) was used to analyze elemental composition, X-ray diffraction (XRD) to identify phase transformations, and scanning electron microscopy coupled with energy-dispersive X-ray spectroscopy (SEM–EDS) to characterize microstructural evolution and elemental distribution. Under the optimized conditions of 15 wt.% coal, 1200 °C, and 60 min, the process produced a magnetic fraction containing 81.31 wt.% Fe, with an Fe recovery of 82.57% and a metallization degree of 87%. Concurrently, the non-magnetic fraction achieved Ti and V recoveries of 83.56% and 85.12%, respectively. The optimized conditions enabled efficient Fe recovery while controlling Ti and V distribution between the magnetic and non-magnetic fractions.

Keywords: Iron Sand; Carbothermic Reduction; Magnetic Separation; Fe-Ti-V

Introduction

Iron sand containing magnetite (Fe_3O_4) and ilmenite ($FeTiO_3$) is a potential source of iron (Fe), titanium (Ti), and vanadium (V) for metallurgical and advanced-material applications [1-2]. Indonesia possesses extensive coastal iron sand deposits, including those in Lampung Province, that offer opportunities for domestic mineral resource development [3]. However, the coexistence of Fe-, Ti-, and V-bearing minerals within complex oxide matrices complicates selective recovery because reduction, diffusion, and mineral phase transformation occur simultaneously during high-temperature processing [4-5]. Carbothermic reduction followed by magnetic separation offers an alternative to conventional smelting, which requires substantial energy input and involves complex metal–slag interactions [2, 6]. This approach promotes the formation of magnetically recoverable metallic Fe while enabling the concentration of Ti-bearing phases in the non-magnetic fraction [3, 6]. Previous studies have achieved high Fe grades using iron sand concentrates and Fe-rich iron sands [3, 6-7], although these results are often associated with feeds containing relatively high initial Fe contents [8-9]. In low-grade iron sand, abundant gangue minerals and Ti-bearing phases can restrict reduction, retain Fe in secondary phases, and impair magnetic separation efficiency [7, 10]. Therefore, process performance must be evaluated not only by Fe recovery but also by the extent of Fe metallization and the partitioning of Ti and V between the magnetic and non-magnetic fractions.

The effectiveness of this process depends on the competition between Fe oxide reduction and the formation or stabilization of secondary silicate and titanate phases [11-12]. Insufficient reduction can leave magnetite and ilmenite incompletely transformed, limiting metallic Fe liberation, whereas more intensive treatment may promote Fe incorporation into secondary phases rather than further metallic Fe formation [13]. These competing reactions are particularly important in low-grade iron sand containing complex magnetite–ilmenite

associations, where phase evolution can simultaneously influence Fe recovery, metallization, and Ti–V partitioning [4, 14]. Although previous studies have investigated reduction conditions and mineral transformations, the combined effects of coal dosage, reduction temperature, and holding time on these interconnected responses remain insufficiently understood. In particular, the relationship between secondary phase formation, metallic Fe grain growth, and the simultaneous recovery of Fe, Ti, and V has not been adequately established for this feed type. Consequently, increasing reduction intensity may improve one performance indicator without improving overall separation selectivity. Clarifying this relationship is essential for identifying operating conditions that release Fe effectively while retaining Ti and V in the non-magnetic fraction.

To address this issue, this study systematically investigates carbothermic reduction followed by magnetic separation of low-grade iron sand, focusing on coal dosage, reduction temperature, and holding time. Process performance is assessed using Fe grade, Fe recovery, and Fe metallization in the magnetic fraction, together with Ti and V recoveries in the non-magnetic fraction [15-16]. X-ray diffraction (XRD) is used to identify mineral phase transformations, while scanning electron microscopy coupled with energy-dispersive X-ray spectroscopy (SEM–EDS) is employed to characterize metallic Fe grain growth and elemental redistribution among metallic, silicate, and titanate phases. The contribution of this study lies in integrating multi-parameter optimization with phase-level and microstructural analysis to explain how secondary phases govern the balance between Fe liberation and Ti–V partitioning. This integrated assessment provides a basis for selecting reduction conditions that improve Fe recovery and metallization while maintaining effective Ti and V recovery in the non-magnetic fraction, supporting more efficient utilization of low-grade polymetallic iron sand.

Materials and Method

Materials

The raw material used in this study was iron sand collected from Krui, Pesisir Barat Regency, Lampung Province, Indonesia. Prior to carbothermic reduction, the feedstock was characterized to determine its initial chemical composition and mineralogical properties. Elemental composition was analyzed using portable X-ray fluorescence (XRF), while the mineral phases were identified by X-ray diffraction (XRD). The results provide a baseline for evaluating changes in elemental distribution and mineral phase evolution during subsequent reduction and magnetic separation. The elemental composition of the raw iron sand is presented in Table 1.

Table 1 Elemental composition of the raw iron sand determined by portable XRF.

Element	Fe	Ti	V	Si	Ca	Al
Content (wt.%)	37.77	4.95	0.25	2.60	2.28	15.15

The oxide-based composition of the iron sand was further analyzed to evaluate the distribution of major valuable elements and gangue constituents. The corresponding oxide composition is presented in Table 2.

Table 2 Chemical composition of the iron sand feed material determined by benchtop XRF.

Oxide	Fe_2O_3	TiO_2	V_2O_5	SiO_2	CaO	Al_2O_3	MgO
Content (wt.%)	62.15	13.38	0.50	15.15	2.14	2.28	2.60

The crystalline phases present in the raw iron sand were identified using X-ray diffraction (XRD). The diffraction pattern is presented in Figure 1, showing that the feed material mainly consists of magnetite (Fe_3O_4) and ilmenite ($FeTiO_3$), accompanied by minor hematite (Fe_2O_3) and enstatite ($MgSiO_3$). The quantitative phase composition obtained from Rietveld refinement of the XRD pattern is provided in Table 3. Vanadium was not detected as an independent

crystalline phase, indicating that V was incorporated within the lattice structure of Fe-bearing minerals, particularly magnetite and ilmenite [3, 17].

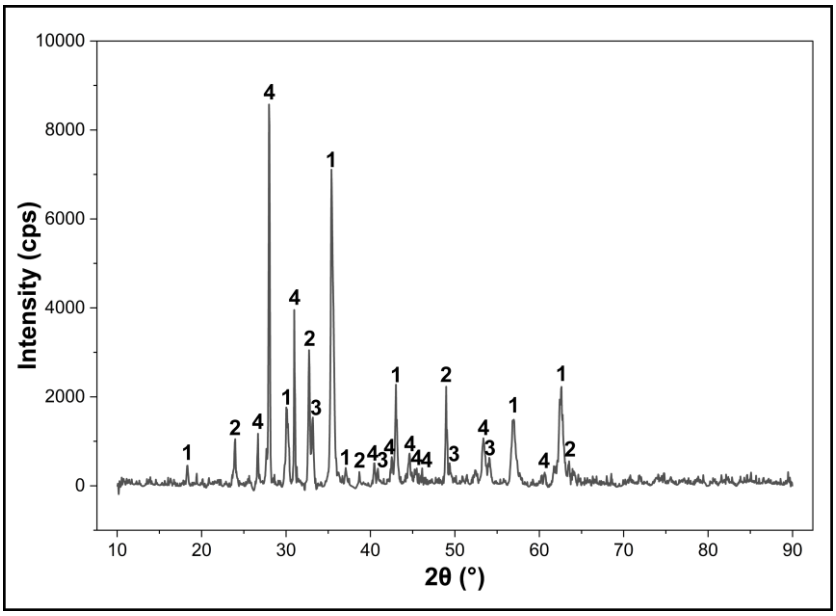


Figure 1 XRD pattern of the iron sand feed material: 1. Magnetite (Fe_3O_4); 2. Ilmenite ($FeTiO_3$); 3. Hematite (Fe_2O_3); 4. Enstatite ($MgSiO_3$)

Table 3 Quantitative phase composition of the raw iron sand.

Phase	Magnetite	Ilmenite	Hematite	Enstatite
Content (wt.%)	19.4	17.6	8.5	54.5

Bituminous coal was used as the carbonaceous reductant during carbothermic reduction. The proximate analysis of coal was conducted on an air-dried basis (adb), and the results are summarized in Table 4 [18]. The coal contained high fixed carbon content, providing the primary reducing agent through carbon gasification and CO generation during reduction [19, 20].

Table 4 Proximate analysis of bituminous coal reductant [18].

Parameter	Moisture	Volatile matter	Ash	Fixed carbon	Sulfur
Content (wt.%)	0.78	21.10	13.55	64.55	2.70

Method

The experimental procedure consisted of carbothermic reduction, phase and microstructural characterization, wet magnetic separation, and melting treatment of the magnetic concentrate. A schematic of the experimental workflow is provided to illustrate the relationships among reduction parameters, phase transformation, and separation performance.

A 40 g portion of raw iron sand was mixed with bituminous coal as the carbonaceous reductant. The coal dosage was set to 10, 15, 20, 25, and 30 wt.% of the iron sand mass. The mixtures were homogenized manually for 30 min to ensure uniform distribution of carbon within the iron sand matrix [21]. The homogenized mixtures were subsequently pelletized into cylindrical pellets with a diameter of 10–15 mm and dried at 120 °C for 4 h to remove moisture prior to reduction.

The dried pellets were placed in graphite crucibles and subjected to carbothermic reduction in a muffle furnace. The effects of reduction temperature and holding time were investigated by varying the reduction temperature from 1000 to 1200 °C and the holding time from 30 to 120 min. The heating rate was maintained at 200 °C h^{-1} for all reduction experiments. A controlled heating rate of 200 °C h^{-1} was applied throughout the reduction experiments to ensure consistent thermal evolution and minimize variations in carbon gasification, CO generation, and reduction kinetics [5]. After reaching the target temperature and completing the predetermined holding period, the reduced pellets were immediately quenched in water to suppress oxidation and preserve the high-temperature phase assemblage formed during reduction [22, 23].

The reduced products were divided into several portions for phase, microstructural, and separation analyses. One portion of the reduced pellet was directly prepared for scanning electron microscopy coupled with energy-dispersive X-ray spectroscopy (SEM–EDS) analysis to evaluate the morphology, grain evolution, and elemental distribution of the Fe-rich phase.

The remaining reduced products were crushed and ground using a vibratory disc mill operated at 950 rpm for 15 min [19]. The ground samples were sieved to a particle size of less than 200 mesh. Approximately 3 g of the sieved powder was analyzed using X-ray diffraction (XRD) to identify crystalline phase transformation during carbothermic reduction.

The remaining ground material was subjected to wet magnetic separation using a Davis Tube tester under a magnetic field intensity of 1500 G, a field strength commonly applied for recovering magnetically susceptible metallic iron from reduced iron sand ore [19, 24]. The magnetic and non-magnetic fractions were collected separately, filtered, dried at 120 °C for 4 h, and weighed to determine mass distribution. The chemical compositions of both fractions were analyzed using X-ray fluorescence (XRF) to evaluate the partitioning behaviors of Fe, Ti, and V during magnetic separation.

The recovery of Fe, Ti, and V was calculated based on the elemental mass distribution between the separated magnetic and non-magnetic fractions [25]. The Fe recovery in the magnetic fraction was calculated using Equation (1).

$$R_{\mathrm{Fe},m} = \left(\frac{\left(G_{\mathrm{Fe},m} \times M_m\right)}{\left(G_{\mathrm{Fe},m} \times M_m\right) + \left(G_{\mathrm{Fe},n} \times M_n\right)} \right) \times 100\% \quad (1)$$

The recoveries of Ti and V in the non-magnetic fraction were calculated using Equation (2).

$$R_{(\mathrm{Ti/V}),n} = \left(\frac{\left(G_{(\mathrm{Ti/V}),NM} \times M_{NM}\right)}{\left(G_{(\mathrm{Ti/V}),m} \times M_m\right) + \left(G_{(\mathrm{Ti/V}),n} \times M_n\right)} \right) \times 100\% \quad (2)$$

where $R_{Fe,m}$ denotes the recovery of Fe in the magnetic fraction, whereas $R_{(Ti/V),n}$ denotes the recovery of Ti or V in the non-magnetic fraction. $G_{Fe,m}$ and $G_{Fe,n}$ represent the Fe grade in the magnetic and non-magnetic fractions, respectively. Similarly, $G_{(Ti/V),m}$ and $G_{(Ti/V),n}$ represent the Ti or V grade in the magnetic and non-magnetic fractions, respectively. M_m and M_n denote the masses of the magnetic and non-magnetic fractions, respectively. The calculated recovery

values were used to quantify the distribution of Fe, Ti, and V between the magnetic and non-magnetic fractions.

The magnetic fraction was further processed by melting to evaluate the formation and composition of the metallic product. A maximum of 15 g of magnetic concentrate was gradually wetted and compacted using a hot-press machine under a 20-ton load for 90 s, then dried at 120 °C for 4 h. The compacted magnetic fraction was melted in a Buehler Arc Melting Furnace equipped with tungsten electrodes under vacuum conditions. Melting was performed at 29.1 V and 152 A, corresponding to a power input of approximately 4.42 kW, under an argon atmosphere maintained at a pressure below 5.0×10^{-2} atm. The resulting metallic product was characterized using a Bruker TASMAN™ Q4 Spark Optical Emission Spectrometer (OES) to determine its chemical composition, while the slag was analyzed by XRF to determine its elemental composition. The Fe metallization degree was determined at the final stage from the ratio of the Fe mass in the metallic product to the initial Fe mass in the iron sand pellets [26]. The Fe mass was calculated from the total mass and Fe grade of each material. The metallization degree was calculated using Equation (3).

$$M_{\mathrm{Fe}} = \left(\frac{m_{\mathrm{Fe},metal}}{m_{\mathrm{Fe},initial}}\right) \times 100\% \quad (3)$$

Where MFe is Fe metallization degree. $m_{Fe,metal}$ represent the mass Fe of the metallic product, and $m_{Fe,initial}$ represent the mass Fe of the initial iron sand pellets. This parameter indicates the proportion of Fe initially contained in the pellets that was recovered as metallic Fe after the whole process [27].

Result and Discussion

Effect of Reductant Dosage

The amount of reductant determines the reducing atmosphere by controlling carbon availability, CO generation, and oxygen removal from iron-bearing minerals [28]. Insufficient

carbon limits the reduction potential and promotes incomplete conversion of Fe oxides, whereas excessive carbon may alter phase stability through secondary reactions and Fe redistribution into stable titanate structures [29]. Therefore, the optimum reductant dosage requires a balance between enhanced Fe oxide reduction and suppression of unfavorable Fe-bearing phases [30]. The effect of coal reductant dosage, varied from 10 to 30 wt.% relative to the ore mass, was evaluated in terms of Fe grade and recovery in the magnetic fraction, Ti and V grades and recoveries in the non-magnetic fraction, and Fe metallization degree.

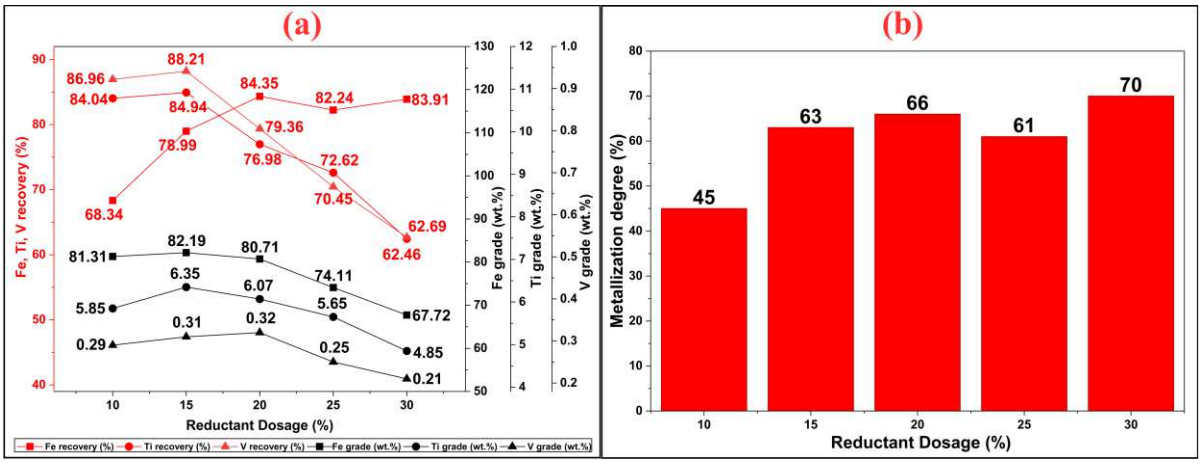


Figure 2 Effect of reductant dosage on:
(a) grade and recovery of Fe, Ti, and V and (b) Fe metallization degree.

At 10 wt.% coal dosage, the reductant supply was insufficient to promote effective reduction of magnetite and ilmenite, as indicated by the low Fe recovery and metallization degree [31]. Increasing the dosage to 15 wt.% substantially improved both parameters, indicating enhanced Fe reduction and liberation. Although Fe recovery reached its maximum at 20 wt.% coal, Ti–V recovery in the non-magnetic fraction declined, suggesting reduced Ti–V partitioning [3, 32]. The degree of Fe metallization tended to plateau above 15 wt.% coal addition, indicating limited additional improvement in Fe reduction. Therefore, 15 wt.% coal was identified as the optimum reductant dosage for promoting Fe reduction while maintaining Ti–V distribution in the non-magnetic fraction. The corresponding phase transformations were further evaluated through XRD analysis to elucidate the effect of coal reductant dosage.

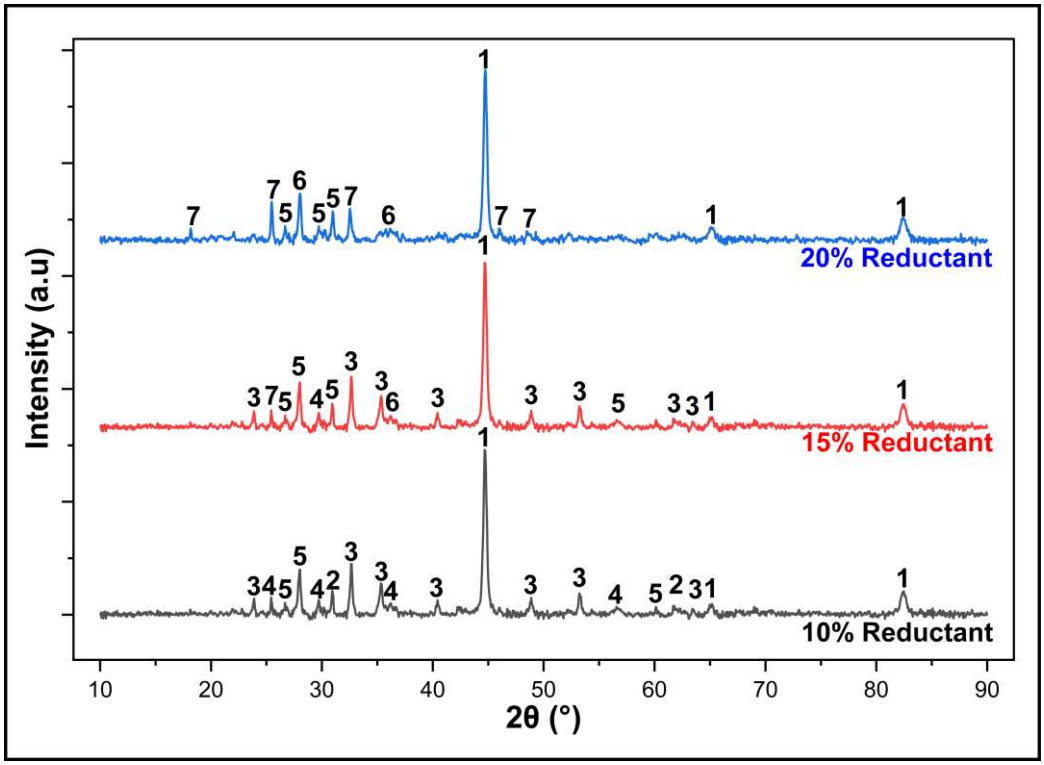


Figure 3 Effect of reductant dosage on phase evolution during carbothermic reduction: 1. Iron (Fe); 2. Magnetite (Fe_3O_4); 3. Ilmenite ($FeTiO_3$); 4. Fayalite (Fe_2SiO_4); 5. Enstatite ($(Mg,Fe)SiO_3$); 6. Pseudobrookite (Fe_2TiO_5); 7. Armalcolite ($(Mg,Fe^{2+})Ti_2O_5$)

The XRD results reveal progressive transformation of Fe- and Ti-bearing minerals with increasing reductant dosage. The observed separation behavior is governed by the progressive transformation of Fe- and Ti-bearing minerals during reduction, as revealed by XRD phase evolution under different reductant conditions. At 10 wt.% coal, the coexistence of magnetite (Fe_3O_4), ilmenite ($FeTiO_3$), and fayalite (Fe_2SiO_4) indicates incomplete Fe oxide reduction and Fe consumption through FeO–SiO_2 interaction, limiting metallic Fe liberation [33]. Increasing coal dosage to 15 wt.% significantly decreased fayalite and increased enstatite ($(Mg,Fe)SiO_3$) formation, indicating preferential incorporation of Mg and Si into the silicate phase rather than Fe-bearing fayalite. This phase evolution may favor Fe recovery by limiting Fe retention in fayalite. However, potential substitution of Mg by Fe in enstatite should be considered, as it may still constrain Fe liberation [34]. At 20 wt.% coal, ilmenite peaks disappeared while enstatite and armalcolite peaks increased, whereas metallic Fe peaks plateaued, indicating that

further ilmenite decomposition promoted Fe incorporation into silicate and titanate structures rather than further Fe liberation [35]. The XRD-observed phase transformation explains the changes in the liberation of metallic Fe and elemental partitioning, as further confirmed by SEM–EDS analysis.

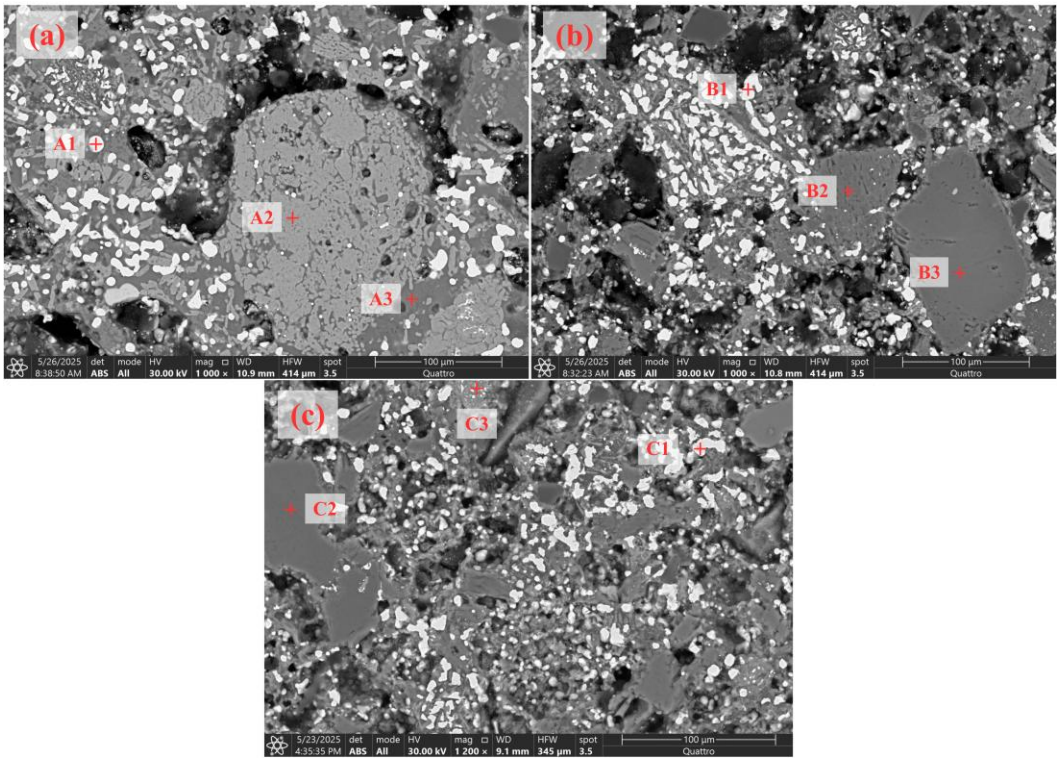


Figure 4 Effect of reductant dosage on microstructural evolution during carbothermic reduction: (a)10 wt.%, (b) 15 wt.%, and (c) 20 wt.%.

Table 5 Effect of reductant dosage on reduced phases by SEM–EDS.

Sample	Phase	Elemental Contents (%)						
		Fe	Ti	V	Mg	Si	O	C
A1	Iron	86.38	1.29	0.03	-	-	-	12.30
A2	Ilmenite	30.75	32.03	0.19	1.62	-	19.81	14.92
A3	Fayalite	16.97	4.92	0.05	1.44	15.02	27.96	24.27
B1	Iron	89.75	1.02	0.04	-	-	-	9.19
B2	Ilmenite	48.23	25.16	0.21	1.86	-	12.88	10.90
B3	Enstatite	15.20	0.75	-	11.70	23.93	31.10	15.34
C1	Iron	91.88	0.78	0.04	-	-	-	7.31
C2	Enstatite	17.32	-	0.01	12.89	24.13	29.16	14.73

C3	Armalcolite	70.93	14.05	0.11	1.96	-	4.29	7.80

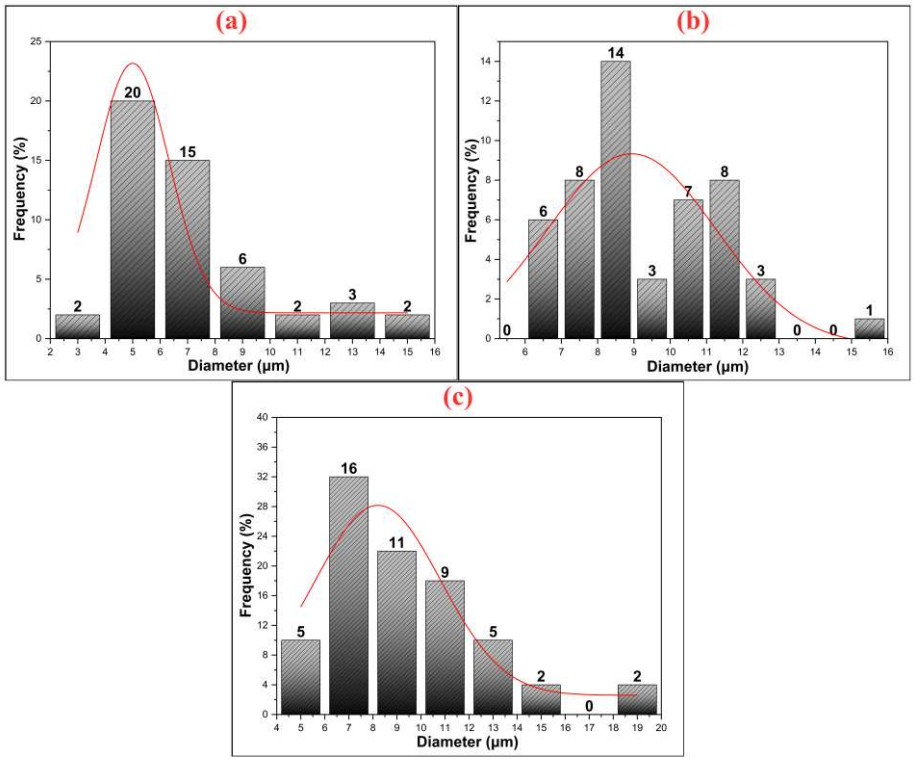


Figure 5 Effect of reductant dosage on the particle size distribution of metallic Fe: (a) 10 wt.%, (b) 15 wt.%, and (c) 20 wt.%.

SEM–EDS analysis revealed that coal reductant dosage governed the morphological evolution, grain growth, and elemental distribution of the metallic Fe phase during carbothermic reduction. At 10 wt.% coal, residual ilmenite and fayalite indicated incomplete reduction and Fe retention in silicate structures. The local Fe content was 86.38 wt.%, with fine metallic Fe grains measuring 4–6 μm, confirming limited grain growth and Fe liberation [22]. Increase to 15 wt.% coal, the local Fe content increased to 89.75 wt.% and grain size reached 8–9 μm, indicating enhanced Fe growth. Residual ilmenite and Fe-bearing enstatite suggest incomplete reduction and limited Fe retention in silicates, while the low Ti content of 0.75 wt.% and undetected V indicate improved elemental separation [4]. At 20 wt.% coal, the local Fe content increased to 91.88 wt.%, while grain size decreased to 6–8 μm. Fe incorporation into enstatite and armalcolite, containing 17.32 wt.% and 70.93 wt.% Fe, respectively, hindered metallic Fe

liberation and grain growth. Although armalcolite promoted Ti–V partitioning, substantial Fe retention made this coal dosage less favorable [35].

The integrated XRF, XRD, and SEM–EDS results identified 15 wt.% coal as the optimum reductant dosage. At 10 wt.%, insufficient reduction favored fayalite formation, whereas 15 wt.% substantially enhanced Fe reduction and liberation while maintaining Ti–V partitioning in the non-magnetic fraction. Increasing the dosage to 20 wt.% promoted Fe incorporation into armalcolite, potentially limiting metallic Fe recovery. However, residual ilmenite at 15 wt.% indicates incomplete phase decomposition, necessitating further process optimization to improve Fe extraction and Ti–V separation.

Effect of Reduction Temperature

The reduction temperature controls reaction kinetics, gas–solid interactions, phase transformations, and the evolution of metallic Fe grains [3]. Insufficient thermal activation limits CO generation and diffusion-controlled reactions, resulting in incomplete reduction of Fe-bearing minerals [36]. In contrast, elevated temperature accelerates oxide conversion and the growth of metallic Fe but may also promote Fe redistribution into thermodynamically stable Ti-bearing phases [5]. Therefore, the applied temperature must balance the enhancement of reduction, the liberation of metallic Fe, and the selective separation of Fe–Ti–V phases. The effect of reduction temperature, varied from 1000 to 1200 °C at a fixed coal reductant dosage of 15 wt.% relative to the ore mass, was evaluated in terms of Fe grade and recovery in the magnetic fraction, Ti and V grades and recoveries in the non-magnetic fraction, and Fe metallization degree.

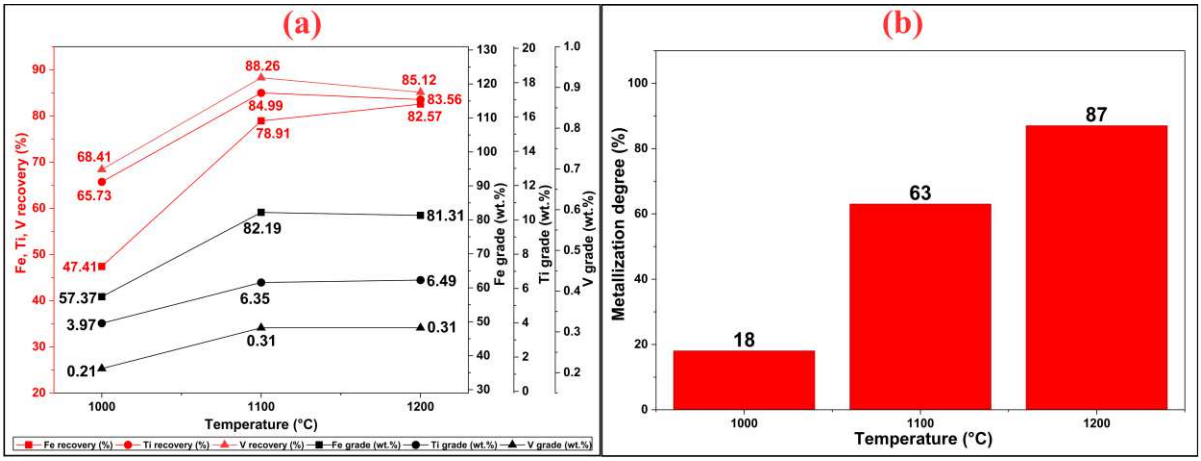


Figure 6 Effect of reduction temperature on:
(a) grade and recovery of Fe, Ti, and V and (b) Fe metallization degree.

At 1000 °C, limited thermal energy restricted the reduction of magnetite and ilmenite, resulting in lower Fe recovery and incomplete Fe metallization [37]. Increasing the temperature to 1100 °C improved Fe, Ti, and V recoveries and significantly increased Fe metallization, indicating enhanced Fe liberation from titanate phases through more effective reduction. At 1200 °C, Fe recovery and Ti–V recovery in the non-magnetic fraction showed a more favorable balance, indicating enhanced oxide decomposition and improved elemental partitioning [8]. The degree of Fe metallization increased continuously with temperature, confirming that higher temperatures promoted Fe reduction. However, 1200 °C was identified as the optimum reduction temperature because it provided a favorable balance between Fe recovery and Ti–V recovery, indicating more effective decomposition of magnetite and ilmenite while maintaining Ti–V partitioning in the non-magnetic fraction [13]. The corresponding temperature-dependent phase transformations were further examined by XRD analysis.

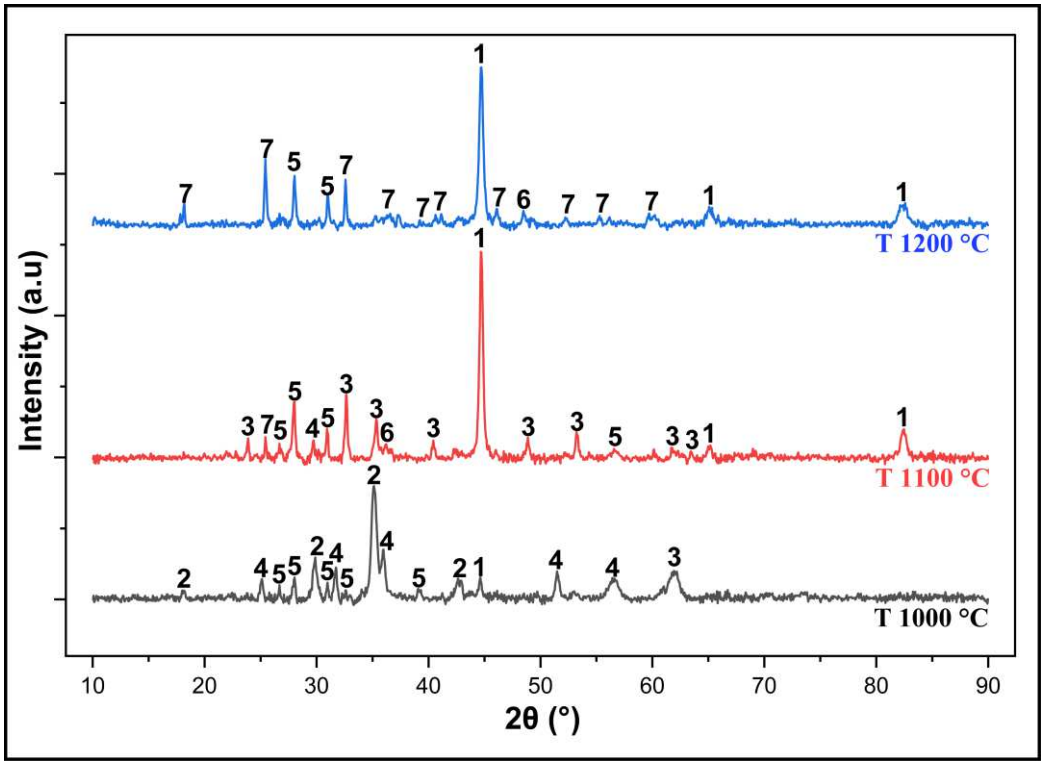


Figure 7 Effect of reduction temperature on phase evolution during carbothermic reduction: 1. Iron (Fe); 2. Magnetite (Fe_3O_4); 3. Ilmenite ($FeTiO_3$); 4. Fayalite (Fe_2SiO_4); 5. Enstatite ($MgSiO_3$); 6. Pseudobrookite (Fe_2TiO_5); 7. Armalcolite ($(Mg,Fe^{2+})Ti_2O_5$)

The XRD results reveal progressive transformations of Fe- and Ti-bearing minerals with increasing reduction temperature, influencing metallic Fe formation and Ti–V partitioning. At 1000 °C, the coexistence of magnetite (Fe_3O_4), ilmenite ($FeTiO_3$), and fayalite (Fe_2SiO_4) indicates incomplete reduction and Fe immobilization through FeO–SiO_2 interactions, thereby limiting metallic Fe liberation [32]. Increasing the temperature to 1100 °C promoted α-Fe formation and eliminated fayalite through preferential MgO–SiO_2 interaction, reducing Fe consumption by iron silicate formation [38]. However, residual ilmenite indicates that titanate decomposition remained incomplete. At 1200 °C, the disappearance of magnetite and ilmenite indicates more extensive reduction and decomposition of the primary Fe- and Ti-bearing minerals. Enstatite ($(Mg,Fe)SiO_3$) formation may limit Fe retention as fayalite, although Fe substitution for Mg in its structure could still restrict Fe liberation. The formation of pseudobrookite (Fe_2TiO_5) and armalcolite ($(Mg,Fe)Ti_2O_5$) further suggests that some Fe

remained incorporated into secondary Fe–Ti-bearing phases [5]. Nevertheless, 1200 °C provided a favorable balance between extensive ilmenite decomposition and preservation of the metallic α-Fe phase. The associated changes in particle morphology and elemental distribution were further examined by SEM–EDS analysis.

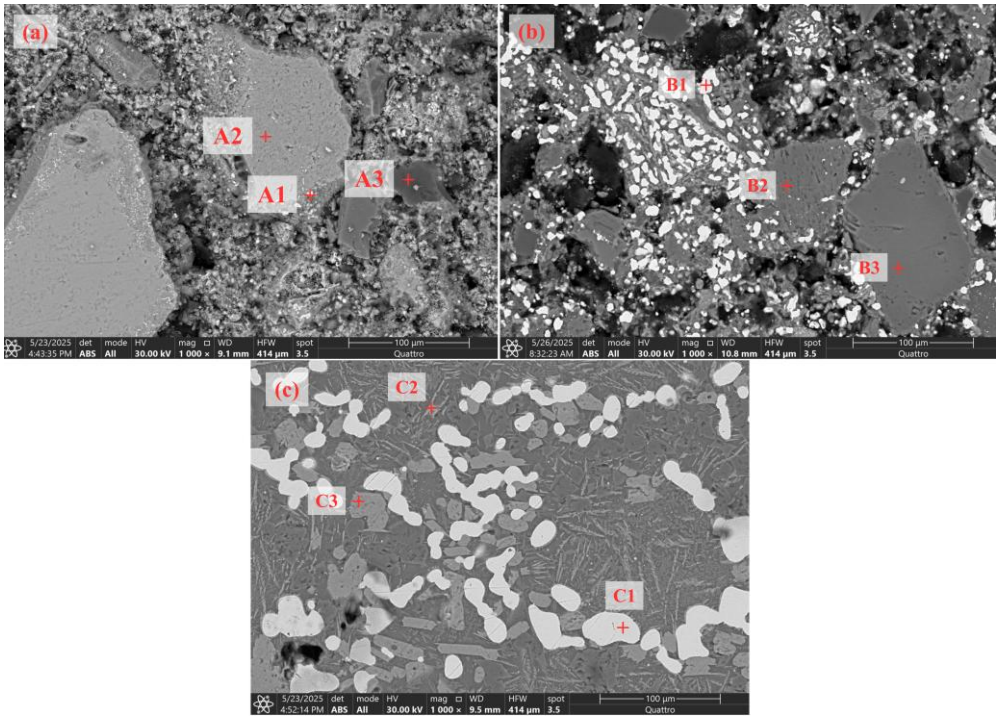


Figure 8 Effect of reduction temperature on microstructural evolution during carbothermic reduction: (a) 1000 °C, (b) 1100 °C, and (c) 1200 °C.

Table 6 Effect of reduction temperature on reduced phases by SEM–EDS.

Sample	Phase	Elemental Contents (%)						
		Fe	Ti	V	Mg	Si	O	C
A1	Iron	71.52	4.17	0.03	-	1.57	6.42	15.72
A2	Ilmenite	44.82	25.42	0.18	1.16	-	16.87	11.55
A3	Fayalite	14.57	-	0.08	7.84	19.43	28.86	27.95
B1	Iron	89.75	1.02	0.04	-	-	-	9.19
B2	Ilemite	48.23	25.16	0.21	1.86	-	12.88	10.90
B3	Enstatite	15.20	0.75	-	11.70	23.93	31.10	15.34
C1	Iron	79.85	-	0.12	-	2.44	0.12	17.89
C2	Pseudobrookite	25.45	10.53	0.08	2.32	10.27	23.85	23.65
C3	Armalcolite	27.87	29.85	0.86	2.22	-	16.76	22.45

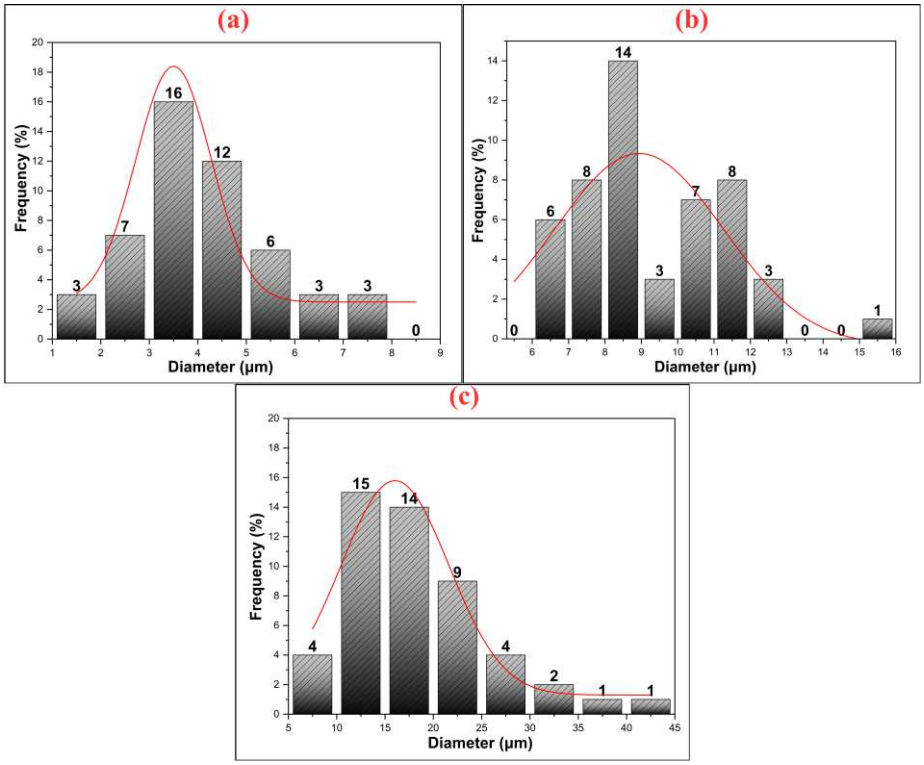


Figure 9 Effect of reduction temperature on the particle size distribution of metallic Fe: (a) 1000 °C, (b) 1100 °C, and (c) 1200 °C.

SEM–EDS analysis revealed that reduction temperature governed the morphological evolution, grain growth, and elemental distribution of the metallic Fe phase during carbothermic reduction [22]. At 1000 °C, the low local Fe content of 71.52 wt.% and elevated Ti content of 4.17 wt.% indicated incomplete reduction. Residual ilmenite containing 44.82 wt.% Fe and 25.42 wt.% Ti, together with fayalite containing 14.57 wt.% Fe, confirmed Fe retention in unreduced titanate and silicate phases. This limited metallic Fe liberation, producing isolated grains of only 3–4 μm and potentially reducing magnetic separation efficiency [4]. Increasing the temperature to 1100 °C, the local Fe content increased to 89.75 wt.% and metallic Fe grains grew to 8–9 μm, indicating improved Fe liberation. However, residual ilmenite containing 48.23 wt.% Fe and 25.16 wt.% Ti, together with Fe-bearing enstatite containing 15.20 wt.% Fe and 0.75 wt.% Ti, confirmed incomplete ilmenite decomposition and continued Fe retention in silicate phases [5]. At 1200 °C, metallic Fe grains grew to 10–15 μm, although the local Fe content decreased to 79.85 wt.% due to Fe partitioning into pseudobrookite containing 25.45

wt.% Fe and armalcolite containing 27.87 wt.% Fe. These titanate phases also concentrated Ti and V, limiting their incorporation into metallic Fe. The coarser grains favor improved liberation during grinding and subsequent magnetic separation [4]. Although increased carbon incorporation may reduce the measured Fe concentration, the improved phase liberation is consistent with the high degree of Fe metallization and favorable Fe–Ti–V separation.

The integrated XRF, XRD, and SEM–EDS results identified 1200 °C as the optimum reduction temperature, providing a favorable balance between metallic Fe grain growth, Fe metallization, and Ti–V separation. At 1000–1100 °C, incomplete mineral reduction restricted Fe liberation, whereas at 1200 °C, extensive ilmenite decomposition and effective separation of Ti-bearing phases supported metallic Fe formation. These findings provided the basis for further optimization of the reduction holding time to promote phase transformation and maintain selective Fe–Ti–V separation.

Effect of Holding Time

Holding time determines the extent of reduction kinetics, phase transformation, and metallic Fe growth by controlling the duration of gas–solid interaction, elemental diffusion, and phase equilibration [25]. Insufficient reaction time restricts CO penetration and limits the conversion of Fe oxide and titanate minerals, resulting in incomplete metallic Fe liberation [39]. Conversely, prolonged holding promotes reduction completion and metallic grain growth but may accelerate secondary phase transformation, leading to Fe redistribution into stable Ti-bearing phases [40]. Therefore, an optimum holding time is required to maximize metallic Fe formation while maintaining selective Fe–Ti–V separation [29]. The effect of holding time, varied from 30 to 120 min under optimized conditions of 15 wt.% coal reductant dosage and a reduction temperature of 1200 °C, was evaluated in terms of Fe grade and recovery in the magnetic fraction, Ti and V grades and recoveries in the non-magnetic fraction, and Fe metallization degree.

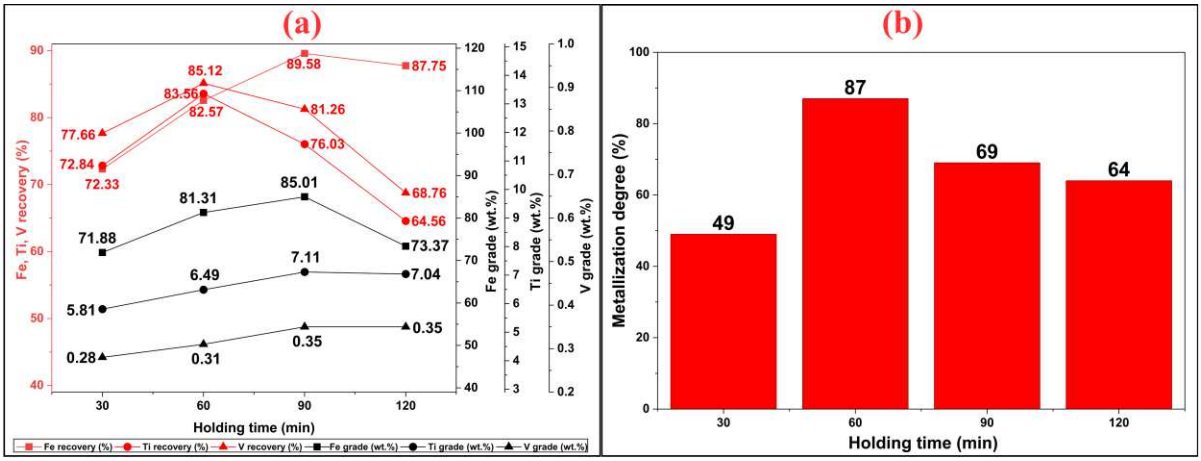


Figure 10 Effect of holding time on:
(a) grade and recovery of Fe, Ti, and V and (b) Fe metallization degree.

At 30 min, low Fe, Ti, and V recoveries indicated incomplete reduction and limited elemental separation. The low Fe metallization degree further confirmed that only a limited proportion of Fe oxides had been converted to metallic Fe [41]. Increasing the holding time to 60 min improved Fe, Ti, and V recoveries and increased Fe metallization, indicating more effective reduction and elemental separation [42]. Extending the holding time beyond 60 min increased Fe recovery but reduced Ti and V recovery in the non-magnetic fraction, while Fe metallization declined significantly. These trends suggest secondary phase formation and elemental redistribution, promoting Ti–V partitioning into the magnetic fraction and limiting metallic Fe formation [45-46]. Therefore, 60 min was identified as the optimum holding time, providing a favorable balance etween Fe reduction, metallic Fe liberation, and Ti–V partitioning [24]. The corresponding phase transformations were further evaluated through XRD analysis to elucidate the effect of holding time.

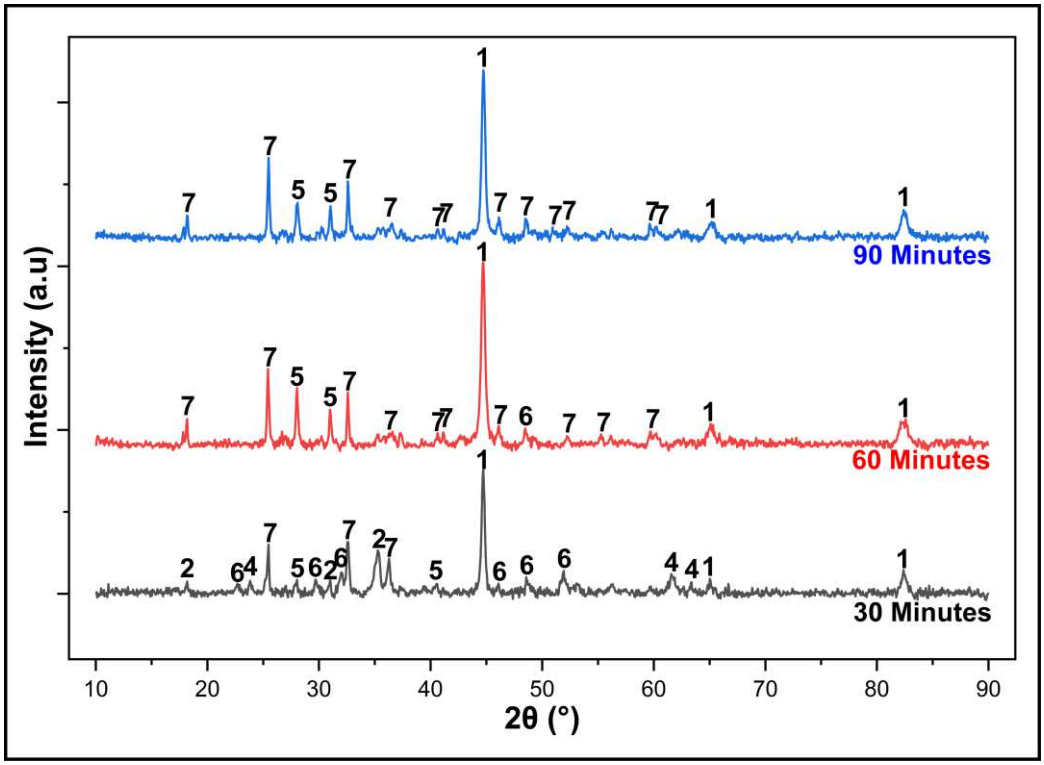


Figure 11 Effect of holding time on phase evolution during carbothermic reduction: 1. Iron (Fe); 2. Magnetite (Fe_3O_4); 3. Ilmenite ($FeTiO_3$); 4. Fayalite (Fe_2SiO_4); 5. Enstatite ($(Mg,Fe)SiO_3$); 6. Pseudobrookite (Fe_2TiO_5); 7. Armalcolite ($(Mg,Fe^{2+})Ti_2O_5$)

The XRD results reveal progressive transformation of Fe- and Ti-bearing minerals with increasing holding time, governing metallic Fe formation and Ti–V partitioning. At 30 min, the formation of pseudobrookite and armalcolite may influence Ti–V partitioning, while residual magnetite indicates that Fe oxide reduction remained incomplete due to insufficient holding time [5]. At a holding time of 60 min, the disappearance of magnetite and ilmenite peaks indicated extensive reduction and decomposition of the primary minerals. The persistence of armalcolite and pseudobrookite suggests that some liberated Fe was incorporated into secondary titanate phases, favoring Ti–V partitioning into the non-magnetic fraction at the expense of Fe recovery [33]. Meanwhile, enstatite formation indicates preferential $MgO–SiO_2$ interaction, limiting Fe consumption through fayalite formation [45]. Although Fe substitution for Mg in enstatite may still limit Fe liberation, this phase assemblage remained favorable for metallic Fe formation. At 90 min, intensified armalcolite peaks indicate increased Ti–V

incorporation into this titanate phase, while declining α-Fe peaks suggest greater Fe sequestration in armalcolite, reducing metallic Fe formation and metallization degree. These results identify 60 min as a favorable holding time for balancing Fe oxide reduction and metallic Fe liberation while maintaining effective Ti–V partitioning into the non-magnetic fraction. The corresponding phase transformations and elemental redistribution were further examined through SEM–EDS analysis.

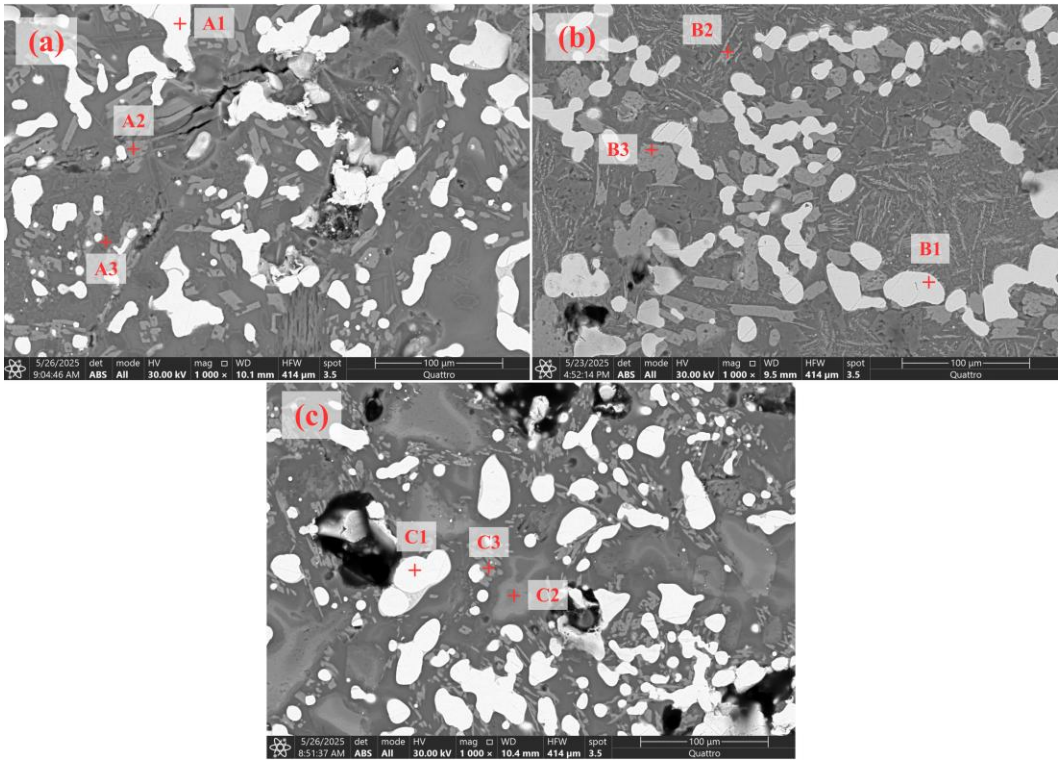


Figure 12 Effect of holding time on microstructural evolution during carbothermic reduction: (a) 30 min, (b) 60 min, and (c) 90 min.

Table 7 Effect of holding time on reduced phases by SEM–EDS.

Sample	Phase	Elemental Contents (%)						
		Fe	Ti	V	Mg	Si	O	C
A1	Iron	76.50	0.21	0.01	-	-	-	23.29
A2	Magnetite	10.52	2.91	-	2.03	15.54	24.09	36.23
A3	Armalcolite	14.28	22.37	0.66	3.27	6.07	15.10	33.95
B1	Iron	79.85	-	0.12	-	2.44	0.12	17.89
B2	Pseudobrookite	25.45	10.53	0.08	2.32	10.27	23.85	23.65

B3	Armalcolite	27.87	29.85	0.86	2.22	-	16.76	22.45
C1	Iron	85.96	0.12	0.02	-	-	-	13.91
C2	Enstatite	8.53	-	0.06	7.93	15.21	24.08	44.07
C3	Armalcolite	4.07	34.47	0.86	3.40	6.45	28.02	17.34

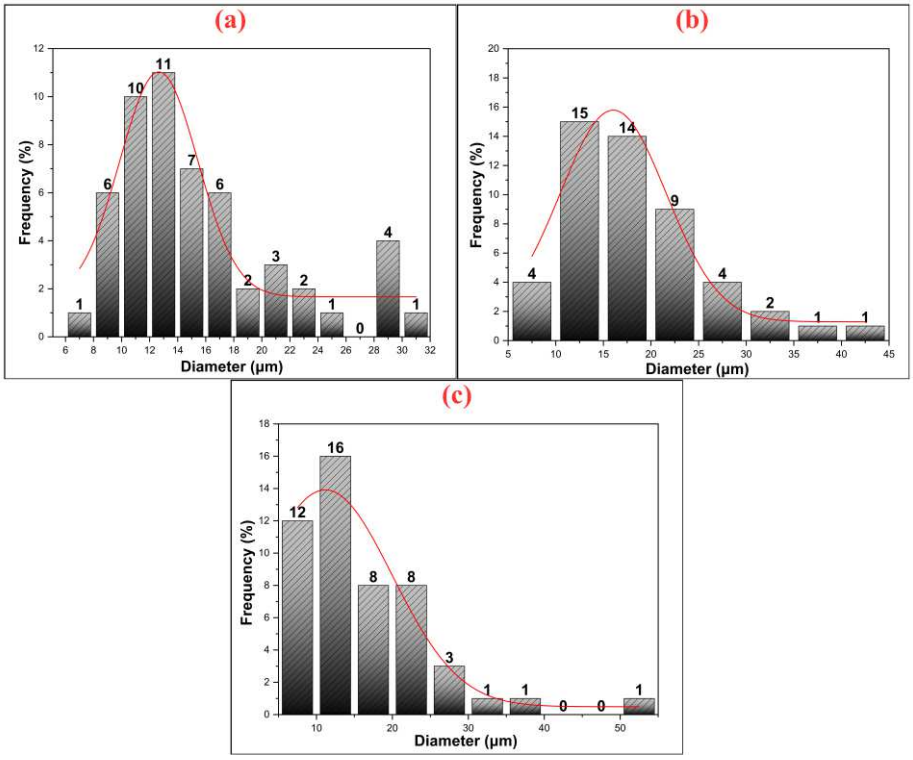


Figure 13 Effect of holding time on the particle size distribution of metallic Fe: (a) 30 min, (b) 60 min, and (c) 90 min.

SEM–EDS analysis revealed that reduction holding time governed the morphological evolution, grain growth, and elemental distribution of the metallic Fe phase during carbothermic reduction [41]. At 30 min, metallic Fe grains measured 10–14 μm with a local Fe content of 76.50 wt.%. Residual magnetite containing 10.52 wt.% Fe indicated incomplete reduction, limiting metallic Fe formation and liberation. metallic Fe reached a local content of 79.85 wt.% with grain sizes of 10–20 μm. The distribution of Ti and V in pseudobrookite and armalcolite, despite partial Fe incorporation, indicates favorable elemental partitioning. The coarser metallic Fe grains may also enhance liberation during grinding and subsequent magnetic separation [46]. At 90 min, the local Fe content increased to 85.96 wt.%, with grain

sizes exceeding 50 μm, potentially enhancing magnetic separation. However, the altered phase distribution suggests less effective Ti–V partitioning, indicating that prolonged holding favored grain coarsening without maintaining selective elemental distribution [34].

The integrated XRF, XRD, and SEM–EDS results identified 60 min as the optimum holding time, providing a favorable balance between metallic Fe growth, phase liberation, and selective Fe–Ti–V separation. At 30 min, incomplete reduction limited metallic Fe formation, whereas extending the holding time to 90 min promoted excessive armalcolite formation, which sequestered Fe in titanate structures, decreased Fe metallization, and impaired Ti–V recovery in the non-magnetic fraction.

Conclusion

The reduction parameters governed Fe liberation, mineral phase transformation, and selective Fe–Ti–V separation during carbothermic reduction followed by magnetic separation. The optimum conditions were 15 wt.% coal reductant, 1200 °C, and 60 min. Under these conditions, the magnetic fraction achieved an Fe grade of 81.31 wt.%, an Fe recovery of 82.57%, and an Fe metallization degree of 87%. Meanwhile, the non-magnetic fraction achieved Ti and V recoveries of 83.56% and 85.12%, respectively, demonstrating effective partitioning of Fe into the magnetic fraction and Ti and V into the non-magnetic fraction. XRD analysis showed extensive decomposition of magnetite and ilmenite at 1200 °C, accompanied by metallic α-Fe formation and changes in iron-bearing silicate and titanate phases. The reduced formation of fayalite limited Fe retention in iron silicates, although enstatite and secondary Fe-bearing titanate phases indicated that some Fe remained incorporated in complex mineral structures. SEM–EDS analysis confirmed metallic Fe grain growth and low Ti incorporation in the analyzed metallic matrix, supporting improved phase liberation and elemental separation. Overall, the combination of 15 wt.% coal, 1200 °C, and 60 min provided the most favorable balance between Fe extraction and Ti–V recovery among the conditions investigated. These

findings demonstrate the potential of carbothermic reduction and magnetic separation to recover Fe selectively while concentrating valuable Ti and V in the non-magnetic fraction, supporting the more efficient utilization of low-grade polymetallic iron sand.

Acknowledgement

The authors gratefully acknowledge the Department of Metallurgical and Materials Engineering, Universitas Indonesia, and the National Research and Innovation Agency (BRIN), Indonesia.

Conflicts of Interest

The authors declare that they have no known financial or non-financial competing interests that could have influenced the work reported in this paper.

Funding

This work was supported in part by the 2026 research grant from the Deputy for Research and Innovation Facilitation and the Research Organization for Nanotechnology and Materials, National Research and Innovation Agency (BRIN), Indonesia.

Author Contribution Statement

Elnando Isaac Latuputty: Conceptualization, Methodology, Resources, Funding acquisition, Writing – original draft & editing. M. Faris Fadillah: Formal analysis, Writing – original draft. Suharto Suharto: Data curation, Formal analysis. Bambang Suharno, Yuliana Sari, and Fajar Nurjaman: Methodology, Validation, Formal analysis, Supervision, Funding acquisition, Writing – review. All authors read and approved the final manuscript.

Data Availability Statement

The data supporting the findings of this study are available from the corresponding author upon reasonable request.

References

[1] Guo K, Wang S, Song R, Zhang Z (2021) Leaching titaniferous magnetite concentrate by alkaline aqueous solution. Min Metall Explor 38:1721–1730. https://doi.org/10.1007/s42461-021-00387-x

[2] Thambiliyagodage C, Wijesekera R, Bakker MG (2021) Leaching of ilmenite to produce titanium based materials: a review. Discov Mater. https://doi.org/10.1007/s43939-021-00020-0

[3] Zulhan Z, Adhiwiguna IBGS, Fuadi A, Saleh N (2021) Solid-state reduction of an Indonesian iron sand concentrate using subbituminous coal. Can Metall Q 60:12–20. https://doi.org/10.1080/00084433.2021.1918508

[4] Salehi H (2021) Phase transitions and microstructural changes during oxidation and reduction of a weathered ilmenite concentrate. Min Metall Explor 38:1167–1173. https://doi.org/10.1007/s42461-021-00397-9

[5] Subasinghe HCS, Ratnayake AS (2025) Thermodynamics, phase transformations, and theoretical perspective of roasting kinetics during sulfurization and carbothermic reduction of ilmenite. Discov Miner 2:5. https://doi.org/10.1007/s44346-025-00010-7

[6] Wijewardhana TPU, Ratnayake AS (2021) Applicability of carbothermic reduction for upgrading Sri Lankan ilmenite ores: towards converting ilmenite into synthetic rutile by mechanical activation. Bull Natl Res Cent. https://doi.org/10.1186/s42269-021-00608-9

[7] Hara RLO, Cook NJ, Lewis EW, Arjomandi M, Brooks G, Chinnici A et al (2025) Thermally assisted beneficiation of a low-grade iron ore powder in a pilot-scale drop tube reactor: effects on ore upgrading, mineralogy and chemical-physical characteristics. Metall Mater Trans B 56:6348–6367. https://doi.org/10.1007/s11663-025-03634-4

[8] Lv W, Elliott R, Lv X, Xiang J, Wang F, Yang Y et al (2021) Generation of titania-rich slag and iron from ilmenite concentrate by carbothermic reduction and magnetic separation in the presence of. Can Metall Q:1–12. https://doi.org/10.1080/00084433.2021.1910427

[9] Zhao Y, Sun T, Wang Z (2021) Extraction of iron from refractory titanomagnetite by reduction roasting and magnetic separation. ISIJ Int 61:93–99. https://doi.org/10.2355/isijinternational.ISIJINT-2020-251

[10] Geldenhuys IJ, Reynolds QG, Akdogan G (2020) Evaluation of titania-rich slag produced from titaniferous magnetite under fluxless smelting conditions. JOM 72:3462–3471. https://doi.org/10.1007/s11837-020-04304-3

[11] Lv X, Lun Z, Yin J, Bai C (2013) Carbothermic reduction of vanadium titanomagnetite by microwave irradiation and smelting behavior. ISIJ Int 53:1115–1119. https://doi.org/10.2355/isijinternational.53.1115

[12] Zhu H, Ma P, Liu C, He J, Yang J (2022) Effect of cryogenic pre-deformation on the stress relaxation response and mechanical / corrosion properties in Al e Zn e Mg e Cu alloy. J Mater Res Technol 20:3471–3484. https://doi.org/10.1016/j.jmrt.2022.08.084

[13] Li X, Kou J, Sun T, Wu S, Zhao Y (2019) Effects of temperature on Fe and Ti in carbothermic reduction of vanadium titanomagnetite with adding MgO. Physicochem Probl Miner Process 55:917–927. https://doi.org/10.5277/ppmp19012

[14] Uwaoma RC, Goso XC, Lekgau KE, Khama MI (2026) Solid-state reduction of titaniferous magnetite ore using coke, anthracite, and charcoal as reductants. Metals 16:479. https://doi.org/10.3390/met16050479

[15] Luo Y, Che X, Wang H, Zheng Q, Wang L (2021) Selective extraction of vanadium from vanadium-titanium magnetite concentrates by non-salt roasting of pellets-H2SO4 leaching process. Physicochem Probl Miner Process 57:36–47. https://doi.org/10.37190/ppmp/138281

[16] Oke EA, Potgieter JH, Nkhoesa D, Van Dyk LD (2025) Vanadium, titanium, and iron extraction from titanomagnetite ore by salt roasting and 21st-century solvents. Separations 12:285. https://doi.org/10.3390/separations12100285

[17] Zulhan Z, Suryani I, Jamali A, Santoso I, Hidayat T (2022) Segregation of iron and titanium in an iron sand concentrate pellet using the isothermal–temperature gradient profile. Min Metall Explor 39:875–883. https://doi.org/10.1007/s42461-022-00576-2

[18] Sari Y, Suharno B, Arham LO, Hakim HZ, Nurjaman F (2026) Gravity-magnetic beneficiation of low-grade iron sand for Fe upgrading and Ti-V enrichment. Period Mineral 95:221–233. https://doi.org/10.13133/2239-1002/19299

[19] Cheng G, Gao Z, Lv M, Yang H, Xue X (2017) Coal-based reduction and magnetic separation behavior of low-grade vanadium-titanium magnetite pellets. Minerals 7:86. https://doi.org/10.3390/min7060086

[20] Zhang Q, Sun Y, Han Y, Li Y, Gao P (2022) Review on coal-based reduction and magnetic separation for refractory iron-bearing resources. Int J Miner Metall Mater 29:2087. https://doi.org/10.1007/s12613-021-2408-x

[21] Hossein A, Meysam S, Sazvar A (2023) Effect of carbon content as reducing agent on the reduction behavior and crushing strength of iron ore composite pellets. Mater Chem Mech 1:24–29. https://doi.org/10.22034/mcm.2023.1.2

[22] Fu Q, Yuan W, Xiang W (2021) Dynamic softening mechanisms and microstructure evolution of TB18 titanium alloy during uniaxial hot deformation. Metals 11:789. https://doi.org/10.3390/met11050789

[23] Nurjaman F, Sari Y, Manurung P, Sapto A (2021) Study of binary, ternary, and quaternary basicity in reduction of saprolitic nickel ore. Trans Indian Inst Met. https://doi.org/10.1007/s12666-021-02391-7

[24] Zhang YM, Yi LY, Wang LN, Chen DS, Wang WJ, Liu YH et al (2017) A novel process for the recovery of iron, titanium, and vanadium from vanadium-bearing titanomagnetite: sodium modification–direct reduction coupled process. Int J Miner Metall Mater 24:504–511. https://doi.org/10.1007/s12613-017-1431-4

[25] Sui Y, Guo Y, Jiang T, Xie X, Wang S, Zheng F (2017) Gas-based reduction of vanadium titano-magnetite concentrate: behavior and mechanisms. Int J Miner Metall Mater 24:10. https://doi.org/10.1007/s12613-017-1373-x

[26] Pintowantoro S, Abdul F, Sanubari F (2020) Study of the effect of binder types on the reduction process and metallurgical properties of Indonesian titanomagnetite iron sand in the point of view of tunnel kiln process. J Chem Technol Metall 56:227–234.

[27] Faris N, Ram R, Tardio J, Bhargava S, McMaster S, Pownceby MI (2017) Application of ferrous pyrometallurgy to the beneficiation of rare earth bearing iron ores – A review. Miner Eng 110:20–30. https://doi.org/10.1016/j.mineng.2017.04.005

[28] Chen F, Li H, Guo Y, Liu K, Wang S, Yang L et al (2025) Reduction disintegration behavior and crystallographic transformation of vanadium–titanium magnetite pellets during hydrogen-based reduction. J Mater Res Technol 34:152–163. https://doi.org/10.1016/j.jmrt.2024.12.021

[29] Chen DS, Song B, Wang LN, Qi T, Wang Y, Wang WJ (2011) Solid state reduction of Panzhihua titanomagnetite concentrates with pulverized coal. Miner Eng 24:864–869. https://doi.org/10.1016/j.mineng.2011.03.018

[30] Mendoza S, Nusheh M, Yin BH, Bumby CW (2025) Comparison of the compressive strength and failure mechanism of hydrogen-reduced iron ore pellets from titanomagnetite ironsand and high-grade magnetite concentrates. Powder Technol 454:120715. https://doi.org/10.1016/j.powtec.2025.120715

[31] Zhao YQ, Sun TC, Zhao HY, Chen C, Wang XP (2019) Effect of reductant type on the embedding direct reduction of beach titanomagnetite concentrate. Int J Miner Metall Mater 26:152–159. https://doi.org/10.1007/s12613-019-1719-7

[32] Zeng R, Wang N, Li W (2021) Influence of SiO2 on the gas-based direct reduction behavior of Hongge vanadium titanomagnetite pellet by hydrogen-rich gases. Powder Technol 386:90–97. https://doi.org/10.1016/j.powtec.2021.03.019

[33] Chandio AD, et al (2023) Beneficiation of low-grade Dilband iron ore by reduction roasting. Metals 13:296. https://doi.org/10.3390/met13020296

[34] Liu YR, Zhang JL, Liu ZJ, Xing XD (2016) Phase transformation behavior of titanium during carbothermic reduction of titanomagnetite ironsand. Int J Miner Metall Mater 23:760–768. https://doi.org/10.1007/s12613-016-1290-4

[35] Vorobkalo NR, Makhambetov YN, Baisanov AS, Zayakin OV (2022) Study of possibility of manufacture of the complex titanium-containing ferroalloy via single-stage carbothermal method. CIS Iron Steel Rev 24:17–23. https://doi.org/10.17580/cisisr.2022.02.03

[36] Li XH, Kou J, Sun TC, Wu SC, Zhao YQ (2020) Effects of calcium compounds on the carbothermic reduction of vanadium titanomagnetite concentrate. Int J Miner Metall Mater 27:301–309. https://doi.org/10.1007/s12613-019-1864-z

[37] She XF, Sun HY, Dong XJ, Xue QG, Wang JS (2013) Reduction mechanism of titanomagnetite concentrate by carbon monoxide. J Min Metall Sect B Metall 49:263–270. https://doi.org/10.2298/JMMB121001020S

[38] Yu W, Wen X, Chen J, Kuang J, Tang Q, Tian Y et al (2017) Preparation of direct reduced iron and titanium nitride from Panzhihua titanomagnetite concentrate through carbothermic reduction-magnetic separation. Minerals 7:220. https://doi.org/10.3390/min7110220

[39] Guo W, Ju J, Luo N, Xing X (2025) Study on the kinetic behavior and mechanism of ilmenite reduction with starch. Metall Mater Trans B 56:4535–4550. https://doi.org/10.1007/s11663-025-03704-7

[40] Chen P, Sun Y, Yang L, Xu R, Luo Y, Wang X et al (2021) Utilization of metallurgy—beneficiation combination strategy to decrease TiO2 in titanomagnetite concentrate before smelting. Minerals 11:1419. https://doi.org/10.3390/min11121419

[41] Zulhan Z, Dinillah R, Yulianton T, Santoso I, Hidayat T (2022) Carbothermic reduction of ilmenite concentrate with sodium carbonate additive to produce iron granules and high titania containing slag. Metals 12:963. https://doi.org/10.3390/met12060963

[42] Guo Y, Zheng Y, Wang S, Xu F, Chen F, Li H et al (2024) Mechanism of iron grains aggregation and growth in metalized pellet under the alternating magnetic fields. J Mater Res Technol 29:3726–3737. https://doi.org/10.1016/j.jmrt.2024.02.122

[43] Wang J, Wen L, Yue D, Zhu F (2026) Evolution behavior of the titanium-bearing phase during the low-temperature fluidized chlorination process of carbonized slag based on microstructure image analysis:1–16. https://doi.org/10.3390/pr14010026

[44] Hammam A, Nasr MI, El-Sadek MH, Omran M, Ahmed A, Li Y et al (2022) Comparative study on the isothermal reduction kinetics of iron oxide pellet fines with carbon-bearing materials. Sustainability 14:8647. https://doi.org/10.3390/su14148647

[45] Joy M, Bhat KH (2025) An overview of phase analysis and strategies on the development of acid soluble titania for sulphate process. Discov Chem. https://doi.org/10.1007/s44371-025-00110-5

[46] Liao J, Zhao B (2022) Phase equilibrium studies of titanomagnetite and ilmenite smelting slags. Int J Miner Metall Mater 29:2162–2171. https://doi.org/10.1007/s12613-021-2376-1